

A Self-Tuning WEC Controller For Changing Sea States ^{*}

Dominic D. Forbush ^{*}, Giorgio Bacelli, Steven J. Spencer,
Ryan G. Coe

^{*} Sandia National Laboratories, Albuquerque, NM 87123 USA (e-mail:
dforbus@ sandia.gov).

Abstract: A self-tuning proportional-integral control law prescribing motor torques was tested in experiment on a three degree-of-freedom wave energy converter. The control objective was to maximize electrical power. The control law relied upon an identified model of device intrinsic impedance to generate a frequency-domain estimate of the wave-induced excitation force and measurements of device velocities. The control law was tested in irregular sea-states that evolved over hours (a rapid, but realistic time-scale) and that changed instantly (an unrealistic scenario to evaluate controller response). For both cases, the controller converges to gains that closely approximate the post-calculated optimal gains for all degrees of freedom. Convergence to near-optimal gains occurred reliably over a sufficiently short time for realistic sea states. In addition, electrical power was found to be relatively insensitive to gain tuning over a broad range of gains, implying that an imperfectly tuned controller does not result in a large penalty to electrical power capture. An extension of this control law that allows for adaptation to a changing device impedance model over time is proposed for long-term deployments, as well as an approach to explicitly handle constraints within this architecture.

Keywords: Wave energy, linear control, self-tuning control, spectral analysis, feedback control

1. INTRODUCTION

Harvesting energy from ocean waves presents a number of technical and practical challenges that must be overcome for this source of renewable energy to be economical. Intelligent control of a wave energy converter (WEC) can significantly enhance power capture and reduce overall cost of energy. Theoretically optimal control of a WEC requires advanced knowledge of the affecting wave (Falnes (2007)). While there is significant focus on accurate future-state wave prediction and prediction-based WEC control strategies (Abdelkhalik et al. (2015), Babarit et al. (2004), Fusco et al. (2010), Coe et al. (2018a)), this architecture remains difficult to implement in practice. The prediction is needed in real-time, which requires either a displaced or remote measurement of incoming waves and an accurate model of wave propagation, or a state-estimation procedure that can be computationally intensive. Both approaches can be confounded in short-crested wave fields, a commonly occurring sea state for which plane-wave approximations are poor wave propagation models (Kimmoun et al. (1999)). Alternatively, approximations of theoretically optimal control that do not require prediction of future waves, but a

frequency-domain estimate of the current sea-state have been pursued (Nguyen and Tona (2017), Bacelli and Coe (2020)). Regardless of architecture, an ideal controller will optimize WEC performance over the changing sea-states to which the device will be subjected. This implies that a control law relying on a spectral estimate of the sea-state must update this estimate over time.

The present work investigates the performance of a proposed simple self-tuning control law in laboratory experiments that adjusts the motor torques of a three degree-of-freedom point absorber in changing sea-states to maximize electrical power capture. The control law uses a spectral estimation of the wave excitation forces that relies on an identified model of device intrinsic impedance. The performance of the control law is considered by comparing the gains resulting from the self-tuning approach to post-calculated optimal gains for a given sea-state. The accuracy of the spectral estimation is considered as well.

2. METHOD

2.1 WaveBot Device

The WaveBot is an axi-symmetric three degree-of-freedom (DOF) point absorber actuated in heave, pitch, and surge (Figure 1). It has identical independent rotary motor/generators on each DOF connected to a common 300V DC bus in the PTO tower. This allows a control force to be applied to the WEC via a belt transmission system (heave and surge) or a driveshaft and a float-contained gearhead (pitch) based upon measurements of velocities in each degree of freedom from shaft-mounted motor encoders

^{*} Sandia National Laboratories is a multi-mission laboratory managed and operated by National Technology and Engineering Solutions of Sandia, LLC., a wholly owned subsidiary of Honeywell International, Inc., for the U.S. Department of Energy's National Nuclear Security Administration under contract DE-NA0003525. This paper describes objective technical results and analysis. Any subjective views or opinions that might be expressed in the paper do not necessarily represent the views of the U.S. Department of Energy or the United States Government.

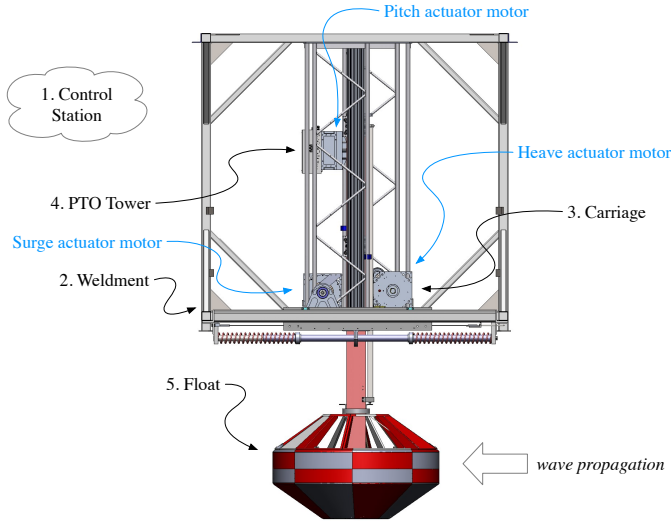


Fig. 1. Simplified diagram of the 3-DOF WaveBot device, axi-symmetric about the z (heave) axis (Bacelli et al. (2019)).

(heave and surge) or an inertial motion unit in the float (pitch). The control system is connected via an EtherCAT network to a Simulink Real-time target computer, so that sensing and control is handled in a Simulink model. The device was tested in the Naval Surface Warfare Center Carderock Maneuvering and Sea-Keeping basin (MASK). Further details regarding device design and testing facility are given in Bacelli et al. (2017), Coe et al. (2018b) and Coe et al. (2019).

2.2 Control Approach

The theoretically optimal power-maximizing control law for an ideal WEC device uses a compensator that is the complex conjugate of the WEC intrinsic impedance, that is, the complex ratio of the device velocity to imposed force at each frequency. The non-causal nature of this controller implies that an estimate of the future input to the device is necessary for implementation on a real system (Falnes (2002)). However, complex conjugate control behavior can be approximated by a feedback controller over a specific range of frequencies (Nevarez et al. (2018)). Since realistic sea-states show excitation over relatively narrow bandwidths, this approximation has practical application. Sea-states also evolve in time: this suggests that the approximated controller must be able to adapt to the given sea state, ideally with no additional sensing. This study proposes a control law that requires only an estimate of device intrinsic impedance and measurements of WEC velocities to maximize device electrical power over all DOFs in changing sea states.

The intrinsic impedance of a WEC follows from the general frequency-domain equations of motion (Falnes (2002)). By simply rearranging and collecting terms, the WEC intrinsic impedance can be defined

$$Z_i(\omega) = i\omega(M + m(\omega)) + B_v + R(\omega) + \frac{S}{i\omega} \quad (1)$$

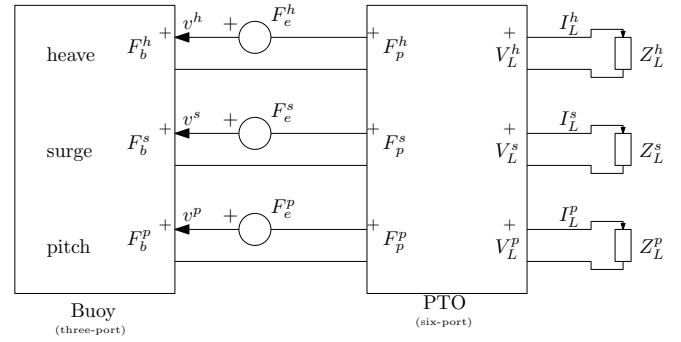


Fig. 2. Multi-Port representation on the WaveBot.

where M and m are the static and added inertia matrices for the device, B_v is the viscous damping matrix, R is the radiation damping matrix, S is the hydrostatic stiffness matrix, and ω is the radian wave frequency. If the device geometry and basic mass properties are known, an estimate of Z_i for a WEC can be estimated from the outputs of a boundary-element method code, excluding viscous damping. In this way, a model of device impedance suitable for initial controller development is available early in the design process.

Development of Device Model Beginning from a high-level model of power flow in the system, the WEC can be modeled as a two-block multi-port circuit (Figure 2) (Coe et al. (2019)). The buoy block captures the hydrodynamic interactions between the device and the wave (forces/torques F , and velocities v), and the power-take-off (PTO) describes the generators. In this model, the electrical power (to be maximized through controller design), is the sum of the powers dissipated on the electrical loads Z_L^h , Z_L^s , and Z_L^p (the product of voltages across V and currents I through each load), where the superscripts h , s , and p indicate the heave, surge and pitch DOFs, respectively. Because each DOF has an independent and identical PTO the six-port model of the PTO becomes diagonal and can be represented as 3 two-port elements between motor force/velocity and quadrature voltage/current,

$$\begin{bmatrix} I_q^i \\ V_q^i \end{bmatrix} = \begin{bmatrix} 0 & (k_t^i n^i)^{-1} \\ k_e^i n^i & r(k_t^i n^i)^{-1} \end{bmatrix} \begin{bmatrix} v^i \\ F_p^i \end{bmatrix}, \quad (2)$$

where i is an index specifying the DOF (h , s , or p) and the parameters k_t^i , k_e^i , n^i and r are the torque constant (Nm/A), electrical constant (Vs/rad), gear ratio, and winding resistance (Ohm) respectively. Due to the identical PTOs, $k_t^i = 6.17$, $k_e^i = 4.12$, and $r = 0.50$ for all DOF, while $n^{h,s} = 12.47$ but $n^p = 3.00$ due to the inclusion of the gearhead on the pitch DOF.

A diagonal proportional-integral controller form was selected due to its broad familiarity,

$$C = \begin{bmatrix} K_p^h + \frac{K_i^h}{s} & 0 & 0 \\ 0 & K_p^s + \frac{K_i^s}{s} & 0 \\ 0 & 0 & K_p^p + \frac{K_i^p}{s} \end{bmatrix}. \quad (3)$$

where s (non-superscript) is the Laplace transform variable. Note that the absence of off-diagonal terms implies

that the controller does not respond to coupling between the surge and pitch degrees of freedom. As shown in Figure 3, the controller uses a measurement of velocity in heave, surge, and pitch to prescribe a force to the motor on each DOF. (A model of the transfer function H relating wave height to excitation force is not needed for controller tuning.)

It can be shown (see Coe et al. (2019) for details), that the electrical power absorbed by the WEC is

$$P_{abs} = \frac{3}{4} \mathcal{R} \left((NK_t)^{-1} C \Omega \right)^* \left((K_e N + R(NK_t)^{-1} C) \Omega \right) \quad (4)$$

where $\Omega = [v^h, v^s, v^p]^T$, the frequency-domain closed-loop model of WEC velocity, and K_t , K_e , R , and N are 3×3 diagonal matrices of parameters $k_t^{h,s,p}$, $k_e^{h,s,p}$, $r^{h,s,p}$, and $n^{h,s,p}$ respectively. In (4), * implies the complex conjugate transpose and script \mathcal{R} implies the real part. By the sign convention of C , $P_{abs} < 0$ for power absorbed by the WEC (that is, power capture is optimized when P_{abs} is as negative as possible).

By simple manipulation of the block diagram (Figure 3), it can further be shown that

$$\Omega = (Z_i - C)^{-1} F_e. \quad (5)$$

Thus, for a given excitation force spectra F_e , and device intrinsic impedance model Z_i (a 3×3 model), the minimum absorbed power P_{abs} is attained for an optimal set of controller gains $\eta_{opt} = \{K_p^h, K_i^h, K_p^s, K_i^s, K_p^p, K_i^p\}$, the result of the optimization

$$\eta_{opt} = \arg \min_{\eta} P_{abs}(\eta, F_e). \quad (6)$$

Using (4) this is solved iteratively in MATLAB via 'fminsearch', recalling that, by sign convention, a minimum of P_{abs} maximizes captured power. With the exception of the first calculation (for which rough order-of-magnitude initial guesses were used), optimal gain estimates from the previous time step are used as the initial guess at the current time step.

Estimation of Excitation Force Equation 6 requires a frequency-domain estimate of the excitation force spectra and a model of device intrinsic impedance. To obtain the latter, the device was subject to multisine excitation in all DOFs, with different phase realizations in each, such that motions in each DOF were approximately uncorrelated. The system identification procedure of Bacelli et al. (2017) was then employed to generate a non-parametric frequency-domain estimate of intrinsic device impedance Z_i , over the frequencies of interest (0.05 to 2 Hz). Considering the simplified linear model (Figure 3), where $inv(Z_i)$ is the inverse of the impedance model, measured WEC velocity spectra, $V(\omega)$, and controller force spectra, $F_{control}(\omega)$, can be used to estimate the excitation force spectra F_e

$$F_e(\omega) = Z_i(\omega)V(\omega) - F_{control}(\omega) \quad (7)$$

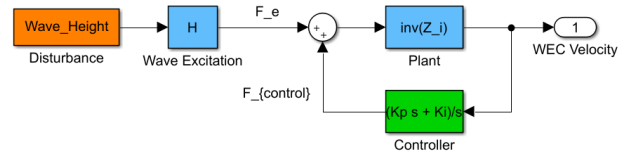


Fig. 3. Block diagram of the linear system model assumed for controller self-tuning. The inverse of the WEC intrinsic impedance Z_i is used as the plant model.

Table 1. Selection of wave ID codes.

Wave ID	Type	T or T_P (s)	H or H_s (m)
2A	JONSWAP	1.58	0.127
10A	JONSWAP	3.5	0.254
CDIP	Data	Varies	Varies

for each DOF. Frequency domain estimates of $V(\omega)$ and $F_{control}(\omega)$ were obtained from real-time experimental time-domain measurements of WEC velocity, $v(t)$, and controller force, $f_{control}(t)$. First, time-domain measurements were down-sampled from 1 kHz to 4 Hz and then a Hamming window was applied to a buffer of 1024 points (i.e., 256 seconds). The Discrete Fourier transform was then applied to this window. Subsequent windows overlap by 1020 points, implying that a Fourier transform is computed each second. Frequencies between 0.15 and 2 Hz are considered in Equation 7, known *a priori* to bound the energy spectra of all selected wave cases (Table 1), such that high-frequency noise or DC-offsets are not included in $F_e(\omega)$ estimations. Spectral estimates were found to be largely insensitive to the extent of down-sampling, overlap, and window length, provided that windows were long enough to estimate the excited frequencies and numerous enough to provide adequate smoothing when averaged.

2.3 Changing Sea-States

The self-tuning control law was tested in variety of changing sea-states. In this work, we focus on two: an approximation of an 'instantaneous' change in sea-state created by abutting two wave time series from distinct irregular sea-states, and a 1/9th Froude-scaled time-series developed from Coastal Data Information Program (CDIP) ocean buoy 225 at the Wave Energy Test site in Kanehoeh Bay, Hawaii. This buoy data was selected as it captures the sea-state evolution during an approaching storm, representing a rapid, though realistic, rate of change. Irregular waves are defined by a JONSWAP spectra with $\gamma = 3.3$ (Hasselmann et al. (1973)), and the shorthand wave ID codes are explained in Table 1.

To evaluate controller performance, each wave case was run a minimum of 2 times. During one of these runs, the WEC was removed from the water. Wave height sensors at the nominal device location were used to characterize the exciting wave field without the influence of device-initiated wave reflections or radiations. This measured wave state can be compared to that estimated (7) to evaluate the performance of the spectral estimator.

3. RESULTS

A comparison between estimated excitation force spectra (7) and excitation force spectra calculated from measured

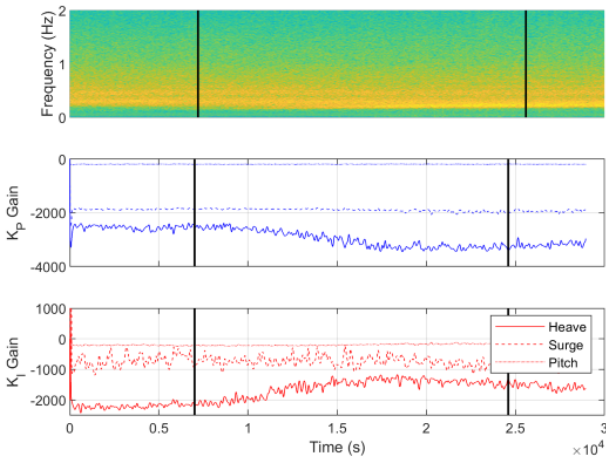


Fig. 4. Self-tuning controller gains for the CDIP225 wave state. Heave, surge, and pitch line styles are consistent across subplots.

wave height spectra at WEC location during the calibration study is calculated as

$$F_{e,actual}(\omega) = H(\omega)\eta(\omega) \quad (8)$$

where H is the identified 1×1 transfer function between input wave height to output excitation force in heave. Of the 3 DOF, heave was selected for this calculation because it consistently showed the largest dynamic responses, resulting in a large signal-to-noise ratio across all sea-states. This estimate from measured wave height is compared to the heave DOF estimate used by the self-tuning controller from (7), which does not use a measurement of wave height or estimate of the excitation model.

To evaluate controller performance, an estimate of excitation force spectra (7) was used to calculate P_{abs} (4) over a dense grid of K_p and K_i gains for each DOF. This allowed a P_{abs} surface to be post-calculated for each sea state. The gains to which the self-tuning controller converged can be compared against the minima of these surfaces to consider the optimality of controller performance for that sea-state.

3.1 CDIP Buoy Sea-State

The spectrogram of wave spectra is shown with time series of controller gains in heave, surge, and pitch to show the adaptation over time (Figure 4). Contrasting wave states at times 7000 s (wave state 1, relatively calm water) and 24600 s (wave state 2, a storm condition) are then examined in detail.

A comparison of the estimated spectra (7) to the actual spectra (8) is given as Figure 5. Estimates for both wave states agree closely: the elevation in spectral energy at the decreased frequency for the second wave state is clearly seen in the estimate, although (7) tends to slightly over-predict excitation force at higher frequencies (0.8 to 1 Hz), where the signal to noise ratios of the terms used in (7) are reduced. The reduced accuracy of the estimation in this range implies in turn that the WEC is less able to absorb power at these higher frequencies, but given the ~ 20 db

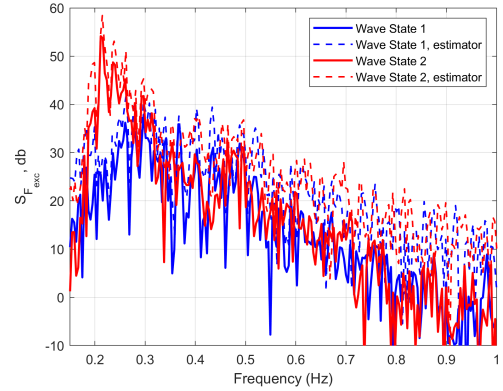


Fig. 5. Estimates of excitation force spectra from wave height measurements (solid lines) and as estimated by the self-tuning controller (dotted lines) for two contrasting wave states in the CDIP225 wave series.

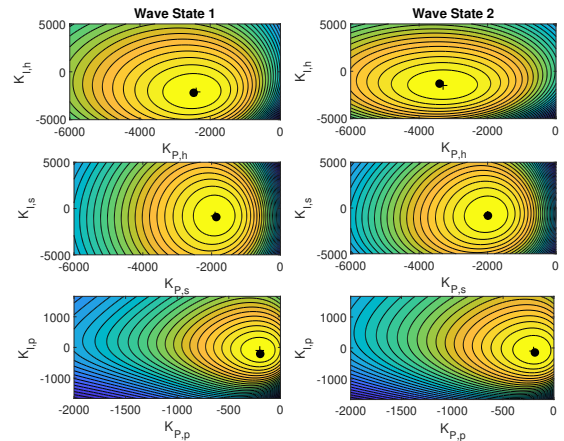


Fig. 6. The WEC power surface as a function of gain tuning for each degree of freedom and wave state for the CDIP 225 wave. Optimal absorbed power is the brightest yellow.

reduction in magnitude at these frequencies, there is little power available.

Figure 6 shows the location of the self-tuning controller gain as the black dot on the post-calculated power surface, and the optimal value of the post-calculated surface as the cross. Because heave is nearly independent from surge and pitch, the heave power surface is described as a function of K_p^h and K_i^h . However, due to the coupling of surge and pitch DOFs, their power surface is four-dimensional (two gains for each DOF). For visualization, a 2D slice was taken of this surface at the optimal surge gains (for the pitch subplot) and the optimal pitch gains (for the surge subplot) such that the self-tuning and optimal controller gains also appear on this slice. Self-tuning gains are near the optimum of the power surface, which indicates a maximized WEC power production, for all degrees of freedom for both wave states. Note that the surface has small gradients near the optimum: this implies both that an optimizer may not reliably converge precisely to the minimum, and that system electrical power is not sensitive to gain selection within this region.

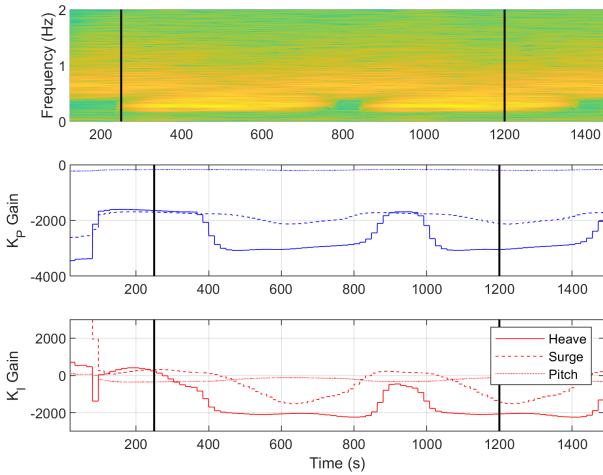


Fig. 7. Self-tuning controller gains for changing 2A-10A wave state. Heave, surge, and pitch line styles are consistent across subplots.

3.2 Concatenated Sea-states

As an example of concatenated wave series, the spectrogram of wave spectra is shown for an alternating wave state 2A to 10A over 5 minute intervals, with time series of controller gains in heave, surge, and pitch to show the adaptation over time (Figure 7). Contrasting wave states at time 250 s and 1200 s are then examined in detail.

Note that in this case, the peak wave period of state 2A is 1.58 s (0.63 Hz), which is nearly the WEC resonant frequency in heave (~ 0.62 Hz). As expected, the K_i^h is near zero during this wave state (at resonance, the optimal K_i gain is zero, (Nguyen and Tona (2017))). The explicitly known transition time of a concatenated wave series allows consideration of the gain adaptation time. The wave state transition is implemented at multiples of 300 s, and the gain adjustment begins approximately 200 s after this. The delay is due to two factors. Firstly, inspection of the spectrogram indicates that the commanded wave transition takes approximately 60 s to manifest in the basin. Second and more significantly, the window length of 256 s will only fully reflect the next sea state after this length of time, and the interim gain will be calculated based upon an average of the two wave states. Accounting for these delay contributions, the gain adapts fairly quickly.

The estimated excitation spectra (not shown) predict excited frequencies well, but again slightly over-estimate amplitudes of higher frequencies ($f > 0.7$ Hz).

The power surfaces for this wave series (Figure 8) indicate that the self-tuning controller gains (dots) are again near the maximum of the post-calculated surface (crosses), which is again flat in the surrounding region, for each wave state and degree of freedom. The largest deviation from the minimum occurs for heave in the first wave state: however, power captured by the self-tuning gains are within 1% of the maximum post-calculated power. The minima location changes more significantly for heave than for surge and pitch, indicating the latter modes to be less sensitive to this changing sea state.

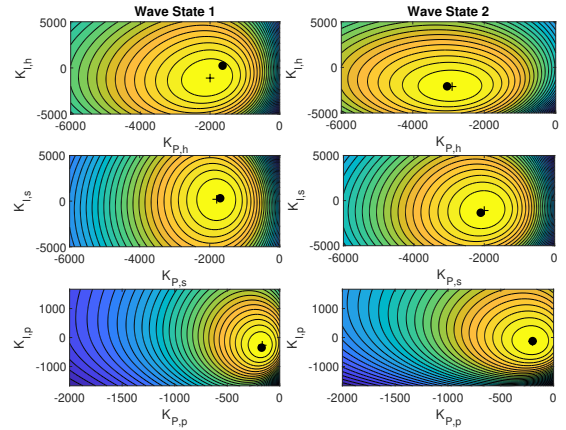


Fig. 8. The WEC power surface as a function of gain tuning for each degree of freedom and wave state for the 2A-10A concatenated wave. Optimum absorbed power is the brightest yellow.

4. DISCUSSION

A six-parameter self-tuning controller was implemented successfully in real-time with 1 KHz sampling on a real-time target machine with two 1.4 GHz processors with a mean execution time of 8.53e-5 seconds: an execution time > 10 times faster than necessary to execute this sampling rate in real time on the small-scale device, which requires faster sampling than an equivalent full-scale device. Gains converged quickly once the buffer from which the spectral estimate was calculated well-approximated the current wave state: particularly for concatenated wave states, the 256 s buffer window appears to significantly delay gain tuning. While it is likely possible to reduce this window time, it is not likely to be necessary in a realistic sea. The present spectral estimate is robust and accurate, and convergence to optimal gains is on the order of minutes. While this is an unallowable delay for sea-states changing on the order of minutes, as in the concatenated wave tests, this is more than adequate for sea states changing over realistic time scales (hours to days), as evidenced particularly by the CDIP225 sea-state investigated in Section 3.

Negative values of K_i provide optimum power capture for sea-states where excitation frequencies are lower than WEC resonance by acting as a negative spring, counteracting hydrostatic restoring stiffness and reducing system resonant frequency. Provided these negative gains do not overcome the hydrostatic stiffness of the device, the system can remain closed-loop stable. This stability bound was not explicitly enforced in the described optimization, and while the tuning procedure never approached instability, incorporating limits on gain values would increase the robustness of the self-tuning controller.

Converged self-tuning gains consistently find the optimal gains for each degree of freedom and wave state. Thus, the performance of the self-tuning controller is commensurate with the PI controllers investigated in Cho et al. (2019a), which attain nearly theoretical limits on performance over a narrow bandwidth, resulting in $\sim 90\%$ power capture compared to optimal complex conjugate control. The flatness of the electrical power surface near the optimal gain

selection in all examined wave cases suggests that this may be a robust feature of this device that is not likely to vary significantly with wave state, and the electrical power production is not particularly sensitive to gain selection. Further, electrical power may be somewhat insensitive to minor modeling errors.

With regard to software implementation, in order to run in real-time, the optimization must converge before the spectra are updated. This somewhat limits the potential gain adjustment time. Further, if the optimization problem is not convex, convergence over any reasonable interval may not be ensured in real-time. In this instance, a look-up table correlating pre-calculated gains to the estimated sea-state could instead be employed. While selected gains cannot be proven to be globally optimal, they can be selected to deliver good performance and be attainable on WEC hardware.

While the PI controller relies on feedback, the *fminsearch* gain-tuning procedures (and the suggested table look-up) are open-loop, using the model of device intrinsic impedance. Any inaccuracy in this model, or a change in the system over a long deployment will reduce the efficacy of this method. Assuming the gain optimization problem remains sufficiently convex, this limitation could be addressed by incorporating an extremum-seeking controller using power feedback to adjust model-informed gains to account for modeling error or a change in system impedance over time.

Finally, this control law is fundamentally single-objective and does not explicitly handle constraints. For longer deployments, it is necessary to also limit the structural loads experienced by the device. The magnitude of the loads experienced by the device can be related to the magnitude of the excitation spectra through identifiable transfer functions. This self-tuning control law can be generalized to any convex cost function. For this case, incorporating load-related terms in (6) would broaden control objectives, although the relative weighting between load-mitigating and power-maximizing objectives would likely be determined on a case-by-case basis. With regard to constraints, it has been shown previously (Cho et al. (2019b)) that a “predictionless” model-predictive controller can be tuned to approximate PI control performance while also explicitly handling constraints. While it may be too computationally intensive to be reasonably implemented in real-time, this suggests an additional step to the proposed control law that would use the identified PI control gains to subsequently derive a model-predictive controller that handles relevant constraints.

REFERENCES

- Abdelkhalik, O., Robinett, R., Bacelli, G., Coe, R., Bull, D., Wilson, D., and Korde, U. (2015). Control optimization of wave energy converters using a shape-based approach. In *ASME Power & Energy*. San Diego, CA.
- Babarit, A., Duclos, G., and Clement, A. (2004). Comparison of latching control strategies for a heaving wave energy device in random sea. *Applied Ocean Research*, 26(5), 227–238. doi:10.1016/j.apor.2005.05.003.
- Bacelli, G. and Coe, R.G. (2020). Comments on control of wave energy converters. *IEEE Transactions on Control System Technology*, 1–4. doi:10.1109/TCST.2020.2965916.
- Bacelli, G., Coe, R.G., Patterson, D., and Wilson, D. (2017). System identification of a heaving point absorber: Design of experiment and device modeling. *Energies*, 10(10), 472. doi:10.3390/en10040472.
- Bacelli, G., Spencer, S.J., Patterson, D.C., and Coe, R.G. (2019). Wave tank and bench-top control testing of a wave energy converter. *Applied Ocean Research*, 86, 351 – 366. doi:10.1016/j.apor.2018.09.009.
- Cho, H., Bacelli, G., Nevarez, V., Wilches-Bernal, F., and Coe, R.G. (2019a). Evaluation of predictionless control for wave energy converters. In *Proceedings of the 13th European Wave and Tidal Energy Conference*. Naples, Italy.
- Cho, H., Bacelli, G., and Coe, R.G. (2019b). Model predictive control tuning by inverse matching for a wave energy converter. *Energies*, 12(21), 1–18. doi:10.3390/en12214158.
- Coe, R.G., Bacelli, G., Nevarez, V., Cho, H., and Wilches-Bernal, F. (2018a). A comparative study on wave prediction for WECs. Technical Report SAND2018-10945, Sandia National Laboratories.
- Coe, R.G., Bacelli, G., Spencer, S.J., and Cho, H. (2018b). Initial results from wave tank test of closed-loop WEC control. Technical Report SAND2018-12858, Sandia National Laboratories, Albuquerque, NM.
- Coe, R.G., Bacelli, G., Spencer, S.J., Forbush, D., and Dullea, K. (2019). Advanced WEC dynamics and controls MASK3 test. Technical Report SAND2019-15428, Sandia National Laboratories.
- Falnes, J. (2002). *Ocean Waves and Oscillating Systems*. Cambridge University Press, Cambridge; New York.
- Falnes, J. (2007). A review of wave-energy extraction. *Marine Structures*, 20(4), 185–201. doi:10.1016/j.marstruc.2007.09.001.
- Fusco, F., Gilloteaux, J.C., and Ringwood, J. (2010). A study on prediction requirements in time-domain control of wave energy converters. In *Proceedings of the 8th IFAC Conference on Control Applications in Marine Systems*. International Federation of Automatic Control, Universitat Rostock, Germany. doi:10.3182/20100915-3-DE-3008.00075.
- Hasselmann, K., Barnett, T., Bouws, E., Carlson, H., Cartwright, D., Enke, K., Ewing, J., Gienapp, H., Hasselmann, D., Kruseman, P., et al. (1973). Measurements of wind-wave growth and swell decay during the joint north sea wave project (JONSWAP). *Ergänzungsheft 8-12*.
- Kimmoun, O., Branger, H., and Kharif, C. (1999). On short-crested waves: experimental and analytical investigations. *European Journal of Mechanicals - B/Fluids*, 18(5), 889–930.
- Nevarez, V., Bacelli, G., Coe, R.G., and Wilson, D.G. (2018). Feedback resonating control for a wave energy converter. In *Proceedings of SPEEDAM2018*.
- Nguyen, H.N. and Tona, P. (2017). Continuously adaptive PI control of wave energy converters under irregular sea-state conditions. In *12th European Wave and Tidal Energy Conference (EWTEC)*.